International Journal of Hydrogen Energy 71 (2024) 1134–1141

Contents lists available at ScienceDirect

International Journal of Hydrogen Energy

journal homepage: www.elsevier.com/locate/he

Enhanced hydrogen storage performance of zinc and magnesium cobaltite nanocomposites

Abbas Eslami [a], Salahaddin Abdollah Lachini [a], Morteza Enhessari [b,*]

[a] Department of Inorganic Chemistry, Faculty of Chemistry, University of Mazandaran, P.O. Box 47416-95447, Babolsar, Iran
[b] Fachbereich Biologie, Chemie, Pharmazie, Institut für Chemie und Biochemie-Anorganische Chemie, Freie Universität Berlin, Fabeckstr. 34/36, 14195 Berlin, Germany

ARTICLE INFO

Handling Editor: Prof B Shabani

Keywords:
Zinc cobaltite
Magnesium cobaltite
Nanocomposites
Discharge capacity
Hydrogen storage

ABSTRACT

Renewable and sustainable energies are vital for the near future. Hydrogen, as a clean energy carrier, is a potential candidate for supplying energy in the foreseeable future. Nowadays, hydrogen storage technology has become a significant issue in the energy sector. In this study, $ZnCo_2O_4$/ZnO and $MgCo_2O_4$/MgO nanocomposites have been synthesized using the sol-gel method with stearic acid as a complexing agent. Different analyses were studied to examine the crystal structure, morphology, and physical properties of the as-prepared samples, including X-ray diffraction (XRD), Fourier transforms infrared (FT-IR), field emission scanning electron microscopy (FESEM), diffuse reflectance spectroscopy (DRS), and vibrating sample magnetometer (VSM). Various methods have been utilized for hydrogen storage technology. In a pioneering approach, the electrochemical hydrogen storage of samples was compared by the chronopotentiometry technique in KOH (4 M) electrolyte solution. The results reveal that $ZnCo_2O_4$/ZnO and $MgCo_2O_4$/MgO nanocomposites exhibit excellent discharge capacities of 4240 and 3529 mAh/g, respectively, after 11 cycles.

1. Introduction

The daily activities of human life, such as industrial, transportation, and residential activities, are carried out using energy. From the lighting of residential buildings to the production of products in factories, all need energy [1]. These energy sources, including oil, natural gas, and coal, are running out soon due to their excessive consumption [2]. It is necessary to find alternative energy sources to meet daily needs. Therefore, the use of renewable energy, such as hydrogen was proposed [3]. It is the most abundant element in nature, the simplest. Hydrogen can be the energy carrier due to having the highest gravimetric energy density, eco-friendly, non-toxic, and has the highest calorific value among all chemical fuels in the future [4]. Hydrogen, as a renewable energy resource, will play a crucial role in sustainable and clean energy systems [5]. Furthermore, it has zero carbon emissions because when hydrogen burns in the air, it produces only water vapor. Hydrogen is superior to other fuels, such as diesel (45%) or gasoline (22%), due to its higher efficiency (60%) and its natural compatibility with fuel cells [6,7]. Researchers have become interested in using hydrogen as a major fuel in the future, so it must be stored safely, low-costly, efficiently, and reversibly. Hydrogen storage systems require a wide range of infrastructure. Hydrogen can be stored in three different phases including gas, solid, and liquid, using various methods, such as liquefied hydrogen in cryogenic tanks (1), cryo-compressed storage (2), compressed gas (3), and solid-state storage (4) [8]. The methods mentioned above (1–3) are not cost-effective due to high costs, safety problems, very low temperatures, and very high pressure. However, the solid-state storage method is superior to the other method mentioned because it does not require high pressure or low temperatures, is safe, cost-effective, and does not need large tanks. In this method, hydrogen can be adsorbed or absorbed onto solid materials through chemisorption or physisorption modes. Additionally, hydrogen molecules migrate inside the lattice of the solid material and physically enter the tiniest and deepest pores [9–11]. So far, several types of compounds have been utilized to store hydrogen, for example, complex hydrides, nanomaterials (nanoparticles, nanocomposites, nanofibers, and nanotubes), polymer nanocomposites, metal-organic frameworks (MOF), and metal hydrides [12–20]. Research on nanomaterials, specifically nanocomposites, has been gaining attention such as transition metal oxides containing Zinc and cobalt, for hydrogen storage materials due to their structural stabilities, surface area-to-volume ratios, and small size for absorbing/releasing hydrogen molecules. Previous studies have

* Corresponding author.
E-mail address: enhessari@zedat.fu-berlin.de (M. Enhessari).

https://doi.org/10.1016/j.ijhydene.2024.05.320
Received 1 February 2024; Received in revised form 9 May 2024; Accepted 20 May 2024
Available online 25 May 2024

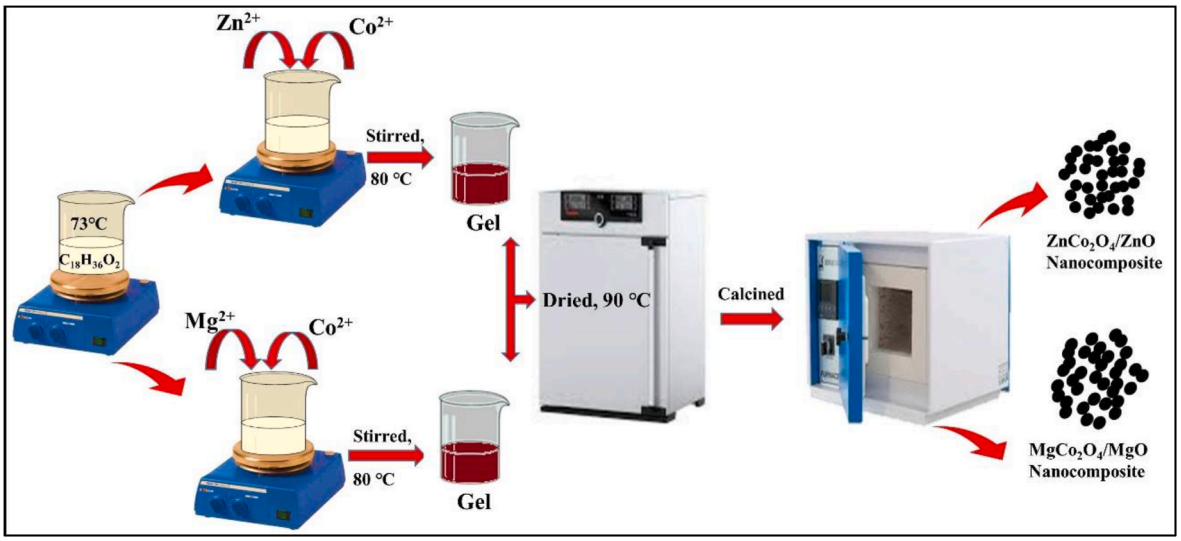

Scheme. 1. Schematic process of the obtained $ZnCo_2O_4$/ZnO and $MgCo_2O_4$/MgO nanocomposites by sol-gel method at 600 °C for 3 h.

reported that nanocomposites such as $Zn_3Mo_2O_9$/ZnO and Co_3O_4–CeO_2 have been utilized for hydrogen storage applications because of their suitable discharge capacity abilities [21–23]. Recent studies on the physio-chemical properties of $ZnCo_2O_4$/ZnO and $MgCo_2O_4$/MgO nanocomposites have shown that these materials exhibit a good cycling lifetime, excellent ion diffusivity, and high specific capacitance [24,25]. These characteristics, make them potentially suitable for use as an electrochemical hydrogen storage material. The leading novelty of this work was the synthesis of $ZnCo_2O_4$/ZnO and $MgCo_2O_4$/MgO nanocomposites using the gel stearic acid method as an application material for hydrogen storage by a simple method and cost-effective. This study aimed to evaluate the impact of nanocomposites in the hydrogen storage process. Therefore, the ability of solid-state composites to absorb and store hydrogen atoms at moderate temperatures and pressure can significantly contribute to the development of hydrogen storage technologies. The measurement and evaluation of hydrogen storage capacity in mixed metal oxides powder using electrochemical methods present several challenges that must be addressed to ensure the reliability and accuracy of results. One limitation lies in the sensitivity of electrochemical techniques, which may struggle to detect subtle changes in hydrogen uptake, particularly at low concentrations. Additionally, variations in the homogeneity of the mixed metal oxides powder can introduce inconsistencies in measurements, impacting the reproducibility of results. Electrode stability over repeated cycles and the kinetics of hydrogen adsorption and desorption processes further complicate accurate evaluation. Temperature and pressure dependencies, alongside the lack of standardized procedures for measurement, pose additional hurdles in achieving reliable data across different experimental setups and laboratories. Surface effects, such as the adsorption of contaminants, also require careful consideration to ensure the integrity of measurements. Addressing these limitations is essential for advancing our understanding of hydrogen storage materials and facilitating their practical applications in various energy storage and conversion technologies. However, to the best of our knowledge, there have been no reports on nanocomposites cobalt $ZnCo_2O_4$/ZnO and $MgCo_2O_4$/MgO for hydrogen storage.

Nowadays, nanocomposite metal oxides are a significant research topic due to their superior physicochemical properties, crystal structure, catalytic abilities, and optical properties than other materials [26]. These materials have extensive applications in various fields, such as medical sciences, energy storage, solar cells, and H_2 sensors [27,28]. Among many synthesized cobalt-containing nanocomposites, $ZnCo_2O_4$/ZnO and $MgCo_2O_4$/MgO nanocomposites have attracted wide attention due to their low cost, abundance, reversible capacity, non-toxicity, and facile synthesis [29,30]. So far, several synthesis approaches, including co-precipitation [31,32], and sol-gel [33,34] have been introduced for the preparation of $ZnCo_2O_4$/ZnO and $MgCo_2O_4$/MgO nanocomposites. In many studies of recent years, cobalt-containing nanocomposites have been used for various applications like photocatalysis [35], supercapacitors [36], and lithium-air batteries [37].

In this study, $ZnCo_2O_4$/ZnO and $MgCo_2O_4$/MgO nanocomposites have been synthesized by a sol-gel method, using stearic acid as a complexing agent. The crystal structure, morphology, and physical properties of the samples were studied using XRD, FT-IR, FESEM, DRS, and VSM analyses. As a novel approach, the electrochemical hydrogen storage performance of the samples was measured and investigated using chronopotentiometry (CP) analysis.

2. Experimental

2.1. Materials and physical measurements

All chemical materials including zinc acetate ($Zn(OAc)_2.2H_2O$), magnesium acetate ($Mg(OAc)_2.4H_2O$), cobalt acetate ($Co(OAc)_2.4H_2O$), and stearic acid were purchased from Merck. X-ray diffraction (XRD) patterns of $ZnCo_2O_4$/ZnO and $MgCo_2O_4$/MgO nanocomposites were studied by a Philips-X'Pert Pro, X-ray diffractometer using Cu Kα radiation. The FTIR spectrum of the samples was recorded with a Shimadzu Varian 4300 spectrophotometer by a KBr pellet technique. The FESEM was employed to study morphology and particle size distribution (FESEM, Mira Tescan 3). A vibrating sample magnetometer was used to measure the magnetic properties of the samples (Meghnatis Daghigh Kavir Co. Kashan, Iran). Ultra-violet-DRS between 220 and 720 nm was employed to study the energy band gap of the compounds (Shimadzu UV/3101 PC). The electrochemical properties of the samples were determined using GC-2550TG (Teif Gostar Faraz Company, Iran).

2.2. Synthesis of $ZnCo_2O_4$/ZnO and $MgCo_2O_4$/MgO nanocomposites

$ZnCo_2O_4$/ZnO nanocomposite was synthesized by the sol-gel method, using Zn^{2+}, Co^{2+} (cation sources), and stearic acid ($C_{16}H_{18}O_2$) as a complexing agent. First, 6 mmol $C_{16}H_{18}O_2$ melted in a beaker at 75 °C. Then, 1 mmol zinc acetate and 2 mmol cobalt acetate were dissolved in distilled water. The solutions containing metallic ions (Zn^{2+}, Co^{2+}) were added to stearic acid and stirred at 70 °C to form a

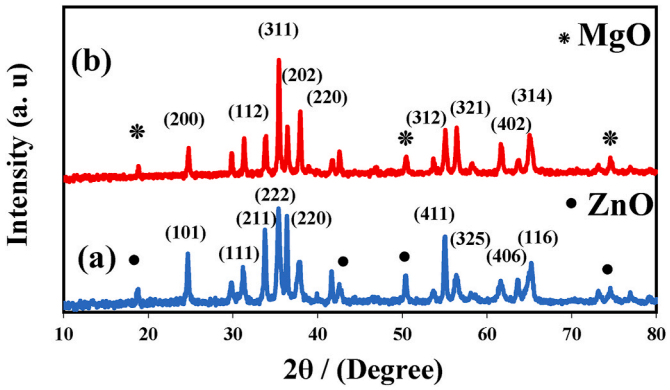

Fig. 1. XRD patterns of (a) $ZnCo_2O_4$/ZnO (b) $MgCo_2O_4$/MgO nanocomposites.

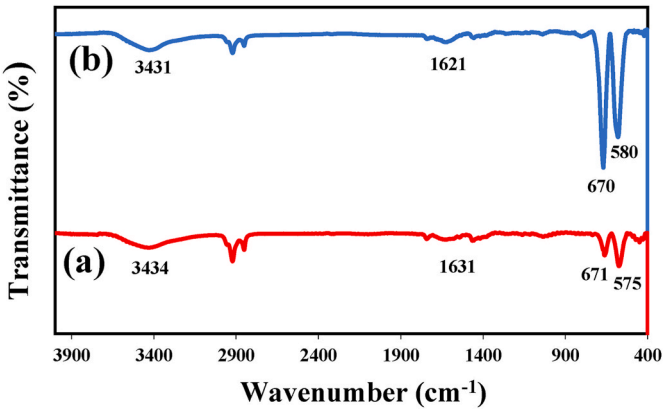

Fig. 2. FTIR spectra of (a) $ZnCo_2O_4$/ZnO (b) $MgCo_2O_4$/MgO nanocomposites.

viscous gel. After cooling the gel at room temperature for 4 h, it was heated in an oven at 90 °C for 12 h to dry. During the drying process of the gel, a homogeneous sol is formed due to the metal cations diffusion from the aqueous phase to the organic phase. Finally, the dried gel was calcined at 600 °C for 3 h to get $ZnCo_2O_4$/ZnO nanocomposites. All the above steps were repeated for the synthesis of $MgCo_2O_4$/MgO nanocomposites (Mg^{2+}: Co^{2+}, 1:2 mmol ratio). Scheme 1 shows a schematic of this procedure.

2.3. Electrochemical studies

The electrochemical hydrogen storage capacities of the $ZnCo_2O_4$/ZnO and $MgCo_2O_4$/MgO nanocomposites was determined using the chronopotentiometry method. A three-electrode cell was employed consisting of a reference electrode (Ag/AgCl), a working electrode (a coated copper sheet), and a counter electrode (platinum). The solution electrolyte (4 M KOH) was prepared by dissolving KOH in deionized water. The constant current (±1 mA) was applied between the working and Pt electrodes, and the potential difference was measured between the working and Ag/AgCl electrodes. The working electrode was made by depositing a thin layer of the as-synthesized samples on the copper sheet (1 × 1 cm^2). $ZnCo_2O_4$/ZnO and $MgCo_2O_4$/MgO nanocomposites were dispersed in ethanol for 20 min. A copper plate was coated with a thin layer of the samples and dried in an electric oven at 80 °C for 25 min.

3. Results and discussion

3.1. XRD analysis

Fig. 1 shows the X-ray diffraction patterns of $ZnCo_2O_4$/ZnO (a) and $MgCo_2O_4$/MgO (b) nanocomposites (b) synthesized using the sol-gel procedure. The XRD diffraction analysis revealed that the $ZnCo_2O_4$/ZnO (JCPDS, 00-023-1390 relating to Zinc cobaltite) and $MgCo_2O_4$/MgO (JCPDS, 00-002-1073 relating to Magnesium cobaltite) nanocomposites have a cubic crystal structure (group Fd-3m) with lattice parameters of a = b = c = 8.1080 and 8.1230 Å, respectively. Additionally, the peak index (major diffractograms) of both samples a and b was observed at 2θ = 37.27° (222) and 36.75° (311), respectively. Elemental analysis reveals the presence of partial amorphous cobalt oxide (Co_3O_4) as the third constituent in every nanocomposite. The average crystallite size of samples was obtained by the Scherrer formula (Eq. 1) [38].

$$D = \frac{0.9\lambda}{\beta \mathrm{Cos}\theta} \quad (1)$$

Where, D is the average crystallite size, λ is the wavelength, β is the FWHM value, and θ is the Bragg angle. The average crystallite size of $ZnCo_2O_4$/ZnO and $MgCo_2O_4$/MgO nanocomposites was obtained to be 12 and 26 nm by the Debye-Scherrer formula, respectively.

3.2. FT-IR analysis

Fig. 2 depicts the infrared spectrum of $ZnCo_2O_4$/ZnO (a) and $MgCo_2O_4$/MgO (b) nanocomposites via the sol-gel method. As shown in Fig. 2, the metal-oxygen bands in both compositions are observed at lower wave numbers than 1000 cm^{-1}. In Fig. 2 (a), two sharp bands at 575-671 cm^{-1} can be related to the Co^{3+}-O^{2-} and Zn^{2+}-O^{2-} (metal-oxygen) bonds [39]. In Fig. 2 (b), the absorption bands at 580-670 cm^{-1} can be attributed to the vibration modes of the metal-oxygen-metal bonds, Mg–O and Co–O [31]. The absorption bands in the range of 1620–1640 cm^{-1} and 3430–3440 cm^{-1} in both compositions suggest the stretching vibration of the O–H group [40].

3.3. FESEM images

The surface morphology of $ZnCo_2O_4$/ZnO (a) and $MgCo_2O_4$/MgO (b) nanocomposites produced by the sol-gel method at 600 °C is shown in Fig. 3(a–d). The morphological results showed distinct differences in distribution, shape, and particle size. The $ZnCo_2O_4$/ZnO (a) and $MgCo_2O_4$/MgO (b) nanocomposites are sphere-like and cubic-shaped, respectively. Additionally, the FESEM images of the samples were investigated using ImageJ software. The histogram of the samples is depicted in Fig. 3(c–d). The average particle size of $ZnCo_2O_4$/ZnO (c) and $MgCo_2O_4$/MgO (d) nanocomposites were obtained to be 32 and 77 nm, respectively.

3.4. VSM studies

The magnetic properties of $ZnCo_2O_4$/ZnO (a) and $MgCo_2O_4$/MgO (b) nanocomposites produced by the sol-gel methods are shown in Fig. 4 (a–b). The hysteresis loops in both compositions confirm the ferromagnetic properties [39,41]. The obtained parameters by using M − H curves like saturation magnetization (Ms), remanence magnetization (Mr), and coercivity (Hc) for both samples are as follows, which show the ferromagnetic properties: $ZnCo_2O_4$/ZnO parameters are Ms. = 0.25 emu/g, Mr. = 0.031 emu/g and Hc = − 200 Oe.

$MgCo_2O_4$/MgO are Ms. = 0.54 emu/g, Mr. = 0.025 emu/g and Hc = − 100 Oe.

3.5. UV-DRS study

The optical properties of $ZnCo_2O_4$/ZnO (a) and $MgCo_2O_4$/MgO (b) nanocomposites synthesized using sol-gel are shown in Fig. 5(a–b). A strong absorption in the visible region is observed at a wavelength of about 340 nm in both samples, which indicates the optical band gap

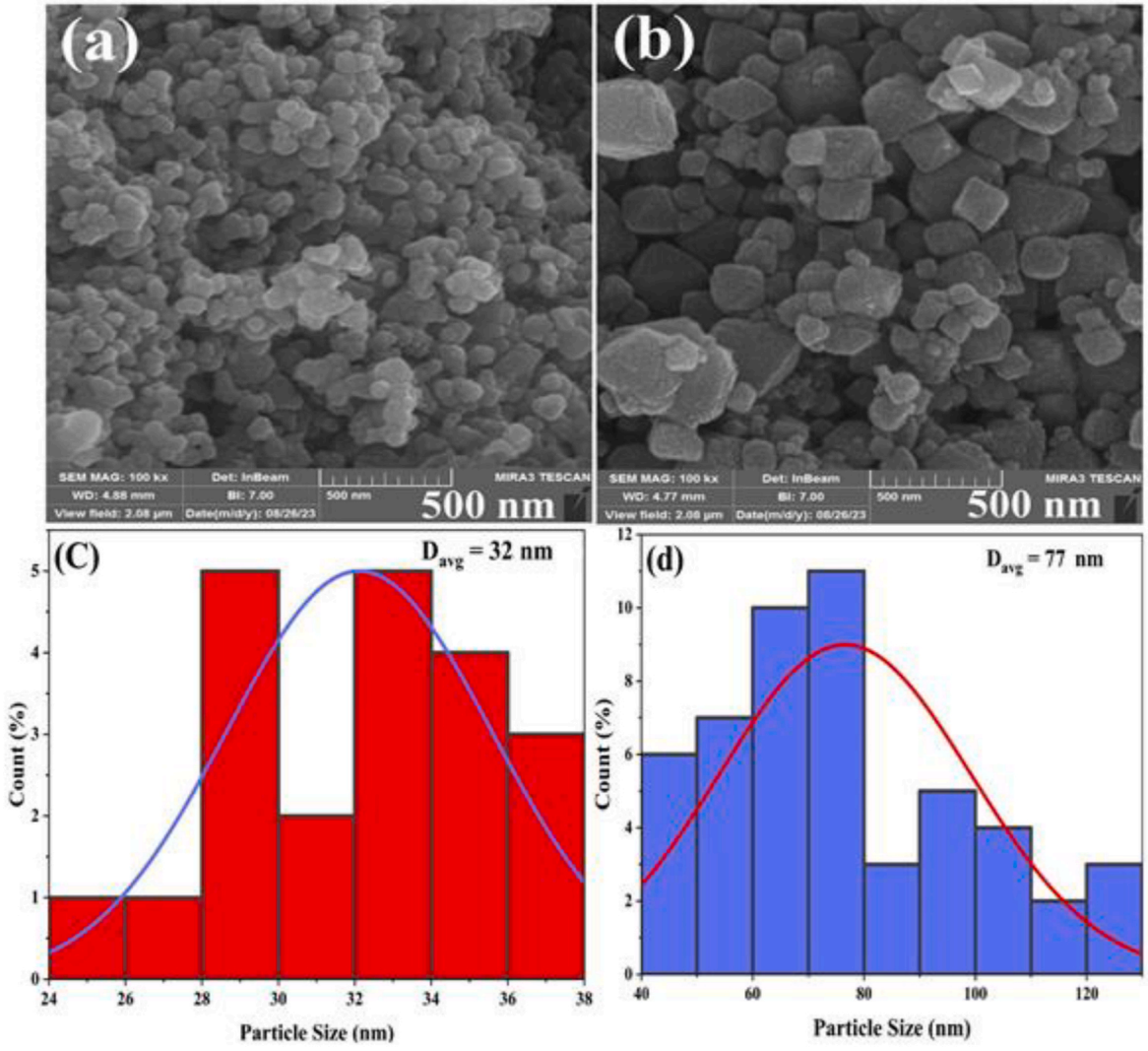

Fig. 3. FESEM images of (a) $ZnCo_2O_4$/ZnO,(b) $MgCo_2O_4$/MgO nanocomposites, and particle size distribution(c-d).

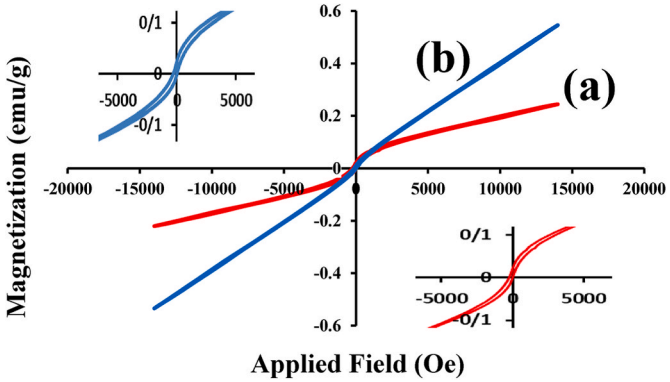

Fig. 4. VSM curves of $ZnCo_2O_4$/ZnO (a) and $MgCo_2O_4$/MgO (b) nanocomposites.

attributed to the O^{2-} (2p) → Co^{3+} (3d) charge-transfer interaction. The optical band gap has been estimated using Tuac's equations (Eq. 2) [2].

$$(\alpha h\upsilon)^n = k\,(h\nu - E_g) \quad (2)$$

Where α is the absorption coefficient, k is the energy-independent constant, n is the nature of transmission, h is the absorption energy, and E_g is the optical band gap. Therefore, the optical band gap for the absorption peak can be obtained by extrapolating the linear portion of the $(\alpha\ h\upsilon)^n$-$h\upsilon$ curve to zero. The band gap energy of $ZnCo_2O_4$/ZnO and $MgCo_2O_4$/MgO nanocomposites was obtained to be 2.6 and 2.4 (eV), respectively.

3.6. Electrochemical properties

Fig. 6 displays the discharge capacity curve of the copper sheet without the.

$ZnCo_2O_4$/ZnO and $MgCo_2O_4$/MgO nanocomposites, which is approximately 3 $mAhg^{-1}$.

Fig. 7 Depicts the electrochemical discharge capacities of (a) $ZnCo_2O_4$/ZnO and (b) $MgCo_2O_4$/MgO electrodes. The discharge capacity of both electrodes is shown in two separate curves over 11 cycles. When a thin layer of the samples is coated onto the copper sheet, the discharge capacity of the electrodes increases. The electrolyte solution was prepared by dissolving KOH in deionized water [42]. During the charging process, hydrogen undergoes adsorption onto the sample surfaces through reductive electron transfer. The accumulation and increase of hydrogen on the surface of the samples leads to the migration of adsorbed H atoms into the interior of the $ZnCo_2O_4$/ZnO and $MnCo_2O_4$/MgO lattice (working electrode) [43]. The electrochemical reactions of the charging process are displayed in equations (3) and (4).

$$H_2O + e^- \rightleftarrows H + OH^- \quad (3)$$

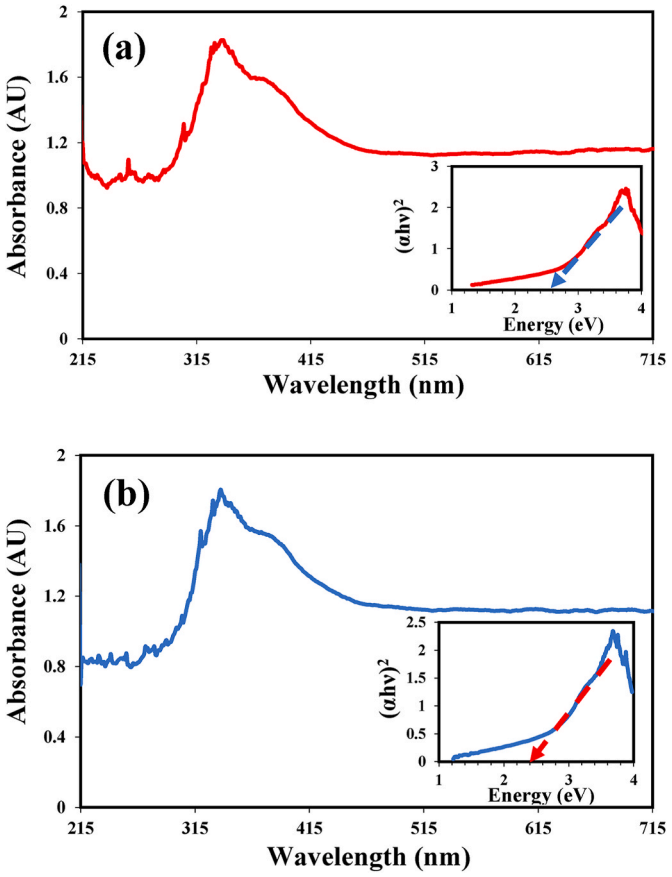

Fig. 5. UV–vis absorption spectrum and the optical energy band gap of (a) $ZnCo_2O_4$/ZnO (b) $MgCo_2O_4$/MgO nanocomposites.

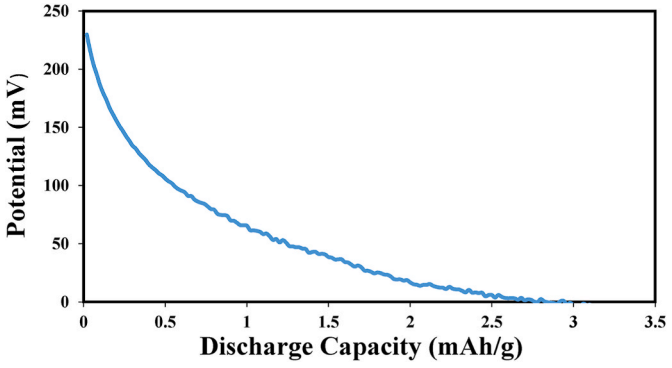

Fig. 6. Diagram of discharge capacity of the blank copper sheet.

$$\text{Samples} + xH_2O + x\,e^- \rightleftarrows (\text{samples -}H_{ads}) + x\,O\,H^- \quad (4)$$

The discharging process happens in the opposite way of the charging procedure, H atoms again convert to water in an alkaline medium (4 M KOH) by generating an electron (Eq. (4)). The significant enhancement in discharge capacity can be related to various factors such as structure, morphology, particle size, and the formation of novel sites for hydrogen desorption/absorption on the surface of the working electrode [14,44]. Also, the physisorption mechanisms for electrochemical hydrogen storage are described, based on the Heyrovsky (Eq. (6)) process and the Tafel reaction (Eqs. (7) and (8)) [23].

$$\text{samples-}H_{ads} + H_2O + e^- \rightleftarrows \text{samples} + H_2 + O\,H^- \quad (6)$$

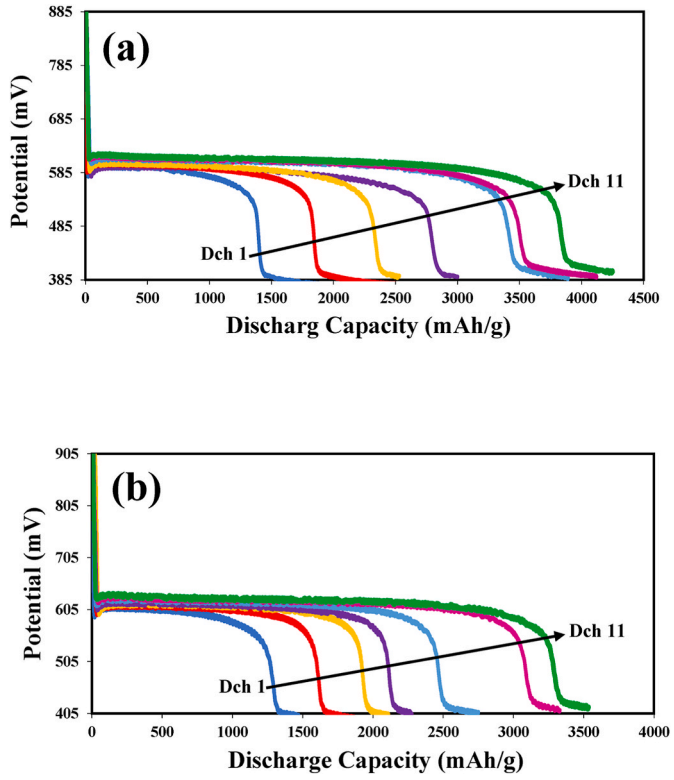

Fig. 7. The discharge curves of (a) Cu–$ZnCo_2O_4$/ZnO and (b) Cu–$MnCo_2O_4$/MgO electrodes at the current (±1 mA).

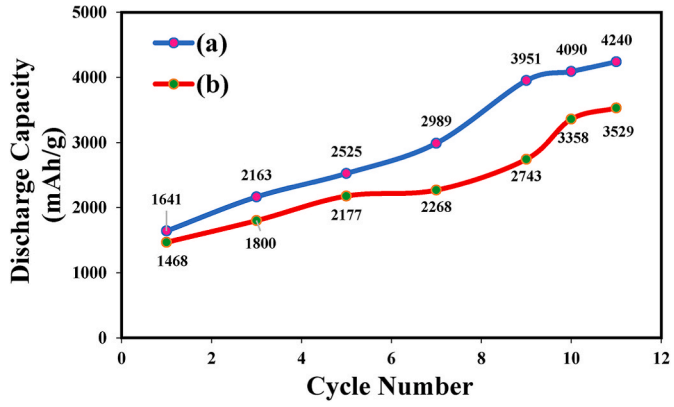

Fig. 8. Cycling performance of (a) $ZnCo_2O_4$/ZnO (b) $MgCo_2O_4$/MgO electrodes at a current of 1 mA.

$$\text{samples-}H_{ads} + \text{samples -}H_{ads} \rightleftarrows 2\,\text{samples} + H_2 \quad (7)$$

$$H + H \rightleftarrows H_2 \quad (8)$$

As shown in Fig. 8, the discharge capacity of $ZnCo_2O_4$/ZnO and $MgCo_2O_4$/MgO nanocomposite enhanced from 1641 to 4240 $mAhg^{-1}$ (maximum discharge) and 1468 to 3529 $mAhg^{-1}$ after 11 cycles, respectively. The surface morphology, higher conductivity, enhanced cycle performance, smaller particle size, and superior ion diffusion properties of the $ZnCo_2O_4$/ZnO nanocomposite, compared to the $MgCo_2O_4$/MgO nanocomposite, can lead to a higher discharge capacity [24]. The amount of hydrogen storage in the discharge cycles can be obtained by the following equation (9) [2].

$$\text{Storage Capacity (SC)} = t_d \times I / m. \quad (9)$$

Table 1
Comparison of the discharge capacity of various materials and as-prepared samples.

Sample	Cycle Number	Discharge Capacity (mAh. g^{-1})	Reference
$NiAl_2O_4$/NiO	15	800	[46]
$ZnGe_2O_4$/graphene	29	2695	[47]
ZnO–CeO_2	20	2400	[48]
$LaCoO_3$/CoO/ La_2O_3	15	1500	[49]
$MgMn_2O_4$	5	2000	[13]
$Dy_2Ce_2O_7$	22	3070	[50]
$ZnCo_2O_4$/ZnO	11	4240	This paper
$MgCo_2O_4$/MgO	11	3529	This paper

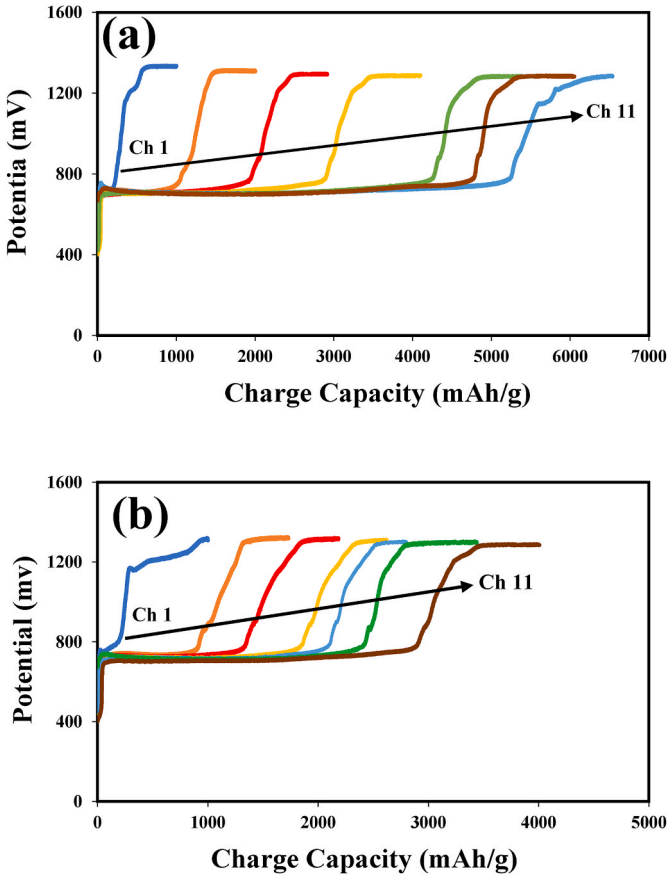

Fig. 9. Charge capacity curves of $ZnCo_2O_4$/ZnO (a) and $MgCo_2O_4$/MgO (b) electrodes after 11 cycles.

where, t_d, I, and m are discharge time (hours), charge/discharge current (mA), and active mass (g), respectively. Generating a double-layer charging process and Faradaic reaction is more than the equilibrium potential, hence, hydrogen can be absorbed/stored [45].

The results show that the $ZnCo_2O_4$/ZnO and $MgCo_2O_4$/MgO nanocomposites can be suitable and promising materials for electrochemical hydrogen storage. Table 1 shows the difference in discharge capacity of the as-synthesized nanocomposites with the previously reported materials.

Fig. 9 displays the charging capacity of the $ZnCo_2O_4$/ZnO (a) and $MgCo_2O_4$/MgO (b) nanocomposite electrodes. According to Fig. 9, by increasing the number of charging cycles, the charging capacity of the electrodes (charging time) has also increased significantly.

4. Conclusions

In this work, $ZnCo_2O_4$/ZnO and $MgCo_2O_4$/MgO nanocomposites were synthesized using the sol-gel method through stearic acid as a complexing agent. The lattice structures of the as-synthesized nanocomposites were identified from XRD patterns. The FTIR results confirmed the formation of metal-oxygen and metal-metal bonds in the samples. The average particle size of $ZnCo_2O_4$/ZnO and $MgCo_2O_4$/MgO nanocomposites 32 and 77 nm were observed in microscopic analysis, respectively. The VSM studies showed the ferromagnetic properties of the samples. The combination of ferromagnetic behavior and high hydrogen storage capacity in the nanocomposites can lead to the development of efficient hydrogen storage materials for hydrogen fuel cell vehicles and portable power applications. These materials could enable compact and lightweight hydrogen storage systems with enhanced storage capacity and faster hydrogen uptake/release kinetics. The UV-DRS analysis revealed that $ZnCo_2O_4$/ZnO and $MgCo_2O_4$/MgO nanocomposites exhibit semiconductor properties, and their band gap energy was estimated to be 2.6 and 2.4 eV, respectively. This band gap energy range is suitable for applications in photovoltaics or photocatalysis. The chronopotentiometry results revealed that the samples have excellent discharge capacity. In particular, the $ZnCo_2O_4$/ZnO nanocomposite (4240 mAh/g) demonstrated a higher hydrogen storage capacity than the $MgCo_2O_4$/MgO nanocomposites (3529 mAh/g). The ability of the samples to efficiently adsorb and store hydrogen at moderate temperatures and pressures could contribute to the development of more efficient and practical hydrogen storage technologies. Therefore, it can be concluded that $ZnCo_2O_4$/ZnO and $MgCo_2O_4$/MgO nanocomposites may be potentially applied for electrochemical hydrogen storage.

Data and code availability

Data will be made available on request.

Ethical approval

No ethical approval was needed for this study.

CRediT authorship contribution statement

Abbas Eslami: Supervision, Project administration, Funding acquisition. **Salahaddin Abdollah Lachini:** Writing – review & editing, Writing – original draft, Validation, Formal analysis, Data curation. **Morteza Enhessari:** Writing – review & editing, Methodology, Conceptualization.

Declaration of competing interest

Conflict of interest the authors declare that they have no known competing financial interests or personal relationships that could have appeared to influence the work reported in this paper.

Acknowledgments

The authors gratefully acknowledge the financial support from the research council of the University of Mazandaran and Freie Universität Berlin.

References

[1] Kaur M, Pal K. Review on hydrogen storage materials and methods from an electrochemical viewpoint. J Energy Storage 2019;23:234–49. https://doi.org/10.1016/j.est.2019.03.020.
[2] Lachini SA, Eslami A. Excellent electrochemical hydrogen storage capabilities of green synthesized $LiCoO_2$ nanoparticles. Int J Hydrogen Energy 2023. https://doi.org/10.1016/j.ijhydene.2023.10.286.

[3] Gholami T, Pirsaheb M. Review on effective parameters in electrochemical hydrogen storage. Int J Hydrogen Energy 2021;46:783–95. https://doi.org/10.1016/j.ijhydene.2020.10.003.

[4] Eslami A, Lachini SA, Shaterian M, Karami M, Enhessari M. Sol-gel synthesis, characterization, and electrochemical evaluation of magnesium aluminate spinel nanoparticles for high-capacity hydrogen storage. J Sol Gel Sci Technol 2023:1–11. https://doi.org/10.1007/s10971-023-06260-1.

[5] Hosseini SE, Wahid MA. Hydrogen production from renewable and sustainable energy resources: promising green energy carrier for clean development. Renew Sustain Energy Rev 2016;57:850–66. https://doi.org/10.1016/j.rser.2015.12.112.

[6] Brown LF. A comparative study of fuels for on-board hydrogen production for fuel-cell-powered automobiles. Int J Hydrogen Energy 2001;26:381–97. https://doi.org/10.1016/S0360-3199(00)00092-6.

[7] Hosseini SE, Butler B. An overview of development and challenges in hydrogen powered vehicles. Int J Green Energy 2020;17:13–37. https://doi.org/10.1080/15435075.2019.1685999.

[8] Esfahani MH, Zinatloo-Ajabshir S, Naji H, Marjerrison CA, Greedan JE, Behzad M. Structural characterization, phase analysis and electrochemical hydrogen storage studies on new pyrochlore $SmRETi_2O_7$ (RE = Dy, Ho, and Yb) microstructures. Ceram Int 2023;49:253–63. https://doi.org/10.1016/j.ceramint.2022.08.338.

[9] Hassan Q, Sameen AZ, Salman HM, Jaszczur M, Al-Jiboory AK. Hydrogen energy future: advancements in storage technologies and implications for sustainability. J Energy Storage 2023;72:108404. https://doi.org/10.1016/j.est.2023.108404.

[10] Yadav S, Oberoi AS, Mittal MK. Electrochemical hydrogen storage: achievements, emerging trends, and perspectives. Int J Energy Res 2022;46:16316–35. https://doi.org/10.1002/er.8407.

[11] Rezayeenik M, Mousavi-Kamazani M, Zinatloo-Ajabshir S. $CeVO_4$/rGO nanocomposite: facile hydrothermal synthesis, characterization, and electrochemical hydrogen storage. Appl Phys A 2023;129:47. https://doi.org/10.1007/s00339-022-06325-y.

[12] Dematteis EM, Amdisen MB, Autrey T, Barale J, Bowden ME, Buckley CE, Cho YW, Deledda S, Dornheim M, de Jongh P, Grinderslev JB, Gizer G, Gulino V, Hauback BC, Heere M, Heo TW, Humphries TD, Jensen TR, Kang SY, Lee Y-S, Li H-W, Li S, Møller KT, Ngene P, Orimo S, Paskevicius M, Polanski M, Takagi S, Wan L, Wood BC, Hirscher M, Baricco M. Hydrogen storage in complex hydrides: past activities and new trends. Prog. Energy. 2022;4:032009. https://doi.org/10.1088/2516-1083/ac7499.

[13] Eslami A, Lachini SA, Shaterian M, Karami M, Enhessari M. Synthesis, characterization, and hydrogen storage capacity of $MgMn_2O_4$ spinel nanostructures. Inorg Chem Commun 2023:110875. https://doi.org/10.1016/j.inoche.2023.110875.

[14] Salehabadi A, Salavati-Niasari M, Gholami T. Green and facial combustion synthesis of $Sr_3Al_2O_6$ nanostructures; a potential electrochemical hydrogen storage material. J Clean Prod 2018;171:1–9. https://doi.org/10.1016/j.jclepro.2017.09.250.

[15] George JK, Yadav A, Verma N. Electrochemical hydrogen storage behavior of Ni-Ceria impregnated carbon micro-nanofibers. Int J Hydrogen Energy 2021;46:2491–502. https://doi.org/10.1016/j.ijhydene.2020.10.077.

[16] Beatrice CAG, Moreira BR, de Oliveira AD, Passador FR, de Almeida Neto GR, Leiva DR, Pessan LA. Development of polymer nanocomposites with sodium alanate for hydrogen storage. Int J Hydrogen Energy 2020;45:5337–46. https://doi.org/10.1016/j.ijhydene.2019.06.169.

[17] Purewal J, Veenstra M, Tamburello D, Ahmed A, Matzger AJ, Wong-Foy AG, Seth S, Liu Y, Siegel DJ. Estimation of system-level hydrogen storage for metal-organic frameworks with high volumetric storage density. Int J Hydrogen Energy 2019;44:15135–45. https://doi.org/10.1016/j.ijhydene.2019.04.082.

[18] Schneemann A, White JL, Kang S, Jeong S, Wan LF, Cho ES, Heo TW, Prendergast D, Urban JJ, Wood BC, Allendorf MD, Stavila V. Nanostructured metal hydrides for hydrogen storage. Chem Rev 2018;118:10775–839. https://doi.org/10.1021/acs.chemrev.8b00313.

[19] Zonarsaghar A, Mousavi-Kamazani M, Zinatloo-Ajabshir S. Sonochemical synthesis of $CeVO_4$ nanoparticles for electrochemical hydrogen storage. Int J Hydrogen Energy 2022;47:5403–17. https://doi.org/10.1016/j.ijhydene.2021.11.183.

[20] Zinatloo-Ajabshir S, Morassaei MS, Amiri O, Salavati-Niasari M, Foong LK. $Nd_2Sn_2O_7$ nanostructures: green synthesis and characterization using date palm extract, a potential electrochemical hydrogen storage material. Ceram Int 2020;46:17186–96. https://doi.org/10.1016/j.ceramint.2020.03.014.

[21] Samimi F, Ghiyasiyan-Arani M, Salavati-Niasari M, Alwash SW. A study of relative electrochemical hydrogen storage capacity of active materials based on $Zn_3Mo_2O_9$/ZnO and $Zn_3Mo_2O_9$/$ZnMoO_4$. Int J Hydrogen Energy 2023;48:10070–80. https://doi.org/10.1016/j.ijhydene.2022.11.301.

[22] Heydariyan Z, Monsef R, Salavati-Niasari M. Insights into impacts of Co_3O_4-CeO_2 nanocomposites on the electrochemical hydrogen storage performance of g-C_3N_4: pechini preparation, structural design and comparative study. J Alloys Compd 2022;924:166564. https://doi.org/10.1016/j.jallcom.2022.166564.

[23] Alinavaz S, Ghiyasiyan-Arani M, Dawi EA, Salavati-Niasari M. Sonochemical synthesis, characterization and investigation of the electrochemical hydrogen storage properties of $Ho_3Fe_5O_{12}$/$Mg_2Al(OH)_7$ nanocomposites. J Energy Storage 2023;66:107369. https://doi.org/10.1016/j.est.2023.107369.

[24] Sun J, Li S, Han X, Liao F, Zhang Y, Gao L, Chen H, Xu C. Rapid hydrothermal synthesis of snowflake-like $ZnCo_2O_4$/ZnO mesoporous microstructures with excellent electrochemical performances. Ceram Int 2019;45:12243–50. https://doi.org/10.1016/j.ceramint.2019.03.134.

[25] Chen H, Liu Y, Wu R, Liu X, Liu Y, Xu C. Battery-type and binder-free $MgCo_2O_4$-NWs@NF electrode materials for the assembly of advanced hybrid supercapacitors. Int J Hydrogen Energy 2022;47:15807–19. https://doi.org/10.1016/j.ijhydene.2022.03.068.

[26] Elemike EE, Onwudiwe DC, Wei L, Chaogang L, Zhiwei Z. Noble metal –semiconductor nanocomposites for optical, energy and electronics applications. Sol Energy Mater Sol Cells 2019;201:110106. https://doi.org/10.1016/j.solmat.2019.110106.

[27] Chaudhary V, TalrejaSonu RK, Rustagi S, Walvekar R, Gautam A. High-performance H_2 sensor based on Polyaniline-WO_3 nanocomposite for portable batteries and breathomics-diagnosis of irritable bowel syndrome. Int J Hydrogen Energy 2024;52:1156–63. https://doi.org/10.1016/j.ijhydene.2023.08.151.

[28] Rameshbabu R, Koh SP, Ajaijawahar K, Jadoun S, Amalraj J, Yaw CT, Tiong SK, Yusaf T. Enhancement of hydrogen storage performance in cost effective novel g–C_3N_4–MoS_2–$Ni(OH)_2$ ternary nanocomposite fabricated via hydrothermal method. Int J Hydrogen Energy 2024;61:743–53. https://doi.org/10.1016/j.ijhydene.2024.02.305.

[29] Li Y, Chu Y, Li Y, Ma C, Li L. A novel electrochemiluminescence biosensor: inorganic-organic nanocomposite and $ZnCo_2O_4$ as the efficient emitter and accelerator. Sens Actuators, B 2020;303:127222. https://doi.org/10.1016/j.snb.2019.127222.

[30] Shukla PS, Agrawal A, Gaur A, Varma GD. Facile synthesis of mesoporous $MnCo_2O_4$@MoS_2 nanocomposites for asymmetric supercapacitor application with excellent prolonged cycling stability. J Energy Storage 2023;59:106580. https://doi.org/10.1016/j.est.2022.106580.

[31] Bhagwan J, Krishna BNV, Yu JS. Facile synthesis of $MgCo_2O_4$ hexagonal nanostructure via co-precipitation approach and its supercapacitive properties. Int J Energy Res 2022;46:7788–98. https://doi.org/10.1002/er.7680.

[32] Rani P, Rohilla S, Verma AS. Synthesis and structural characterization of nanocomposites $ZnCo_2O_4$/ZnO prepared by co-precipitation method. Mater Today Proc 2023. https://doi.org/10.1016/j.matpr.2023.11.153.

[33] Palanivel B, Hossain MS, Reddy IN, Abhinav E M, Al-Enizi AM, Ubaidullah M, Macadangdang RR, Shim J. Chemical oxidants (H_2O_2 and persulfate) activated photo-Fenton like degradation reaction using sol-gel derived g-C_3N_4/$ZnCo_2O_4$ nanocomposite. Diam Relat Mater 2022;130:109413. https://doi.org/10.1016/j.diamond.2022.109413.

[34] Vignesh G, Ranjithkumar R, Devendran P, Nallaperumal N, Sudhahar S, Kumar MK. Structural, spectral, and electrochemical investigations of a nitrogen-doped N-rGO/$MgCo_2O_4$ nanocomposite for supercapacitor applications. ChemistrySelect 2023;8:e202203915. https://doi.org/10.1002/slct.202203915.

[35] Sunitha S, Rao AN, Abraham LS. Antibacterial activity of cobalt doped zinc oxide/carbon nano composite and kinetics for the photocatalytic degradation of acid yellow 110. J Pure Appl Microbiol 2015.

[36] Madhu R, Veeramani V, Chen S-M, Manikandan A, Lo A-Y, Chueh Y-L. Honeycomb-like porous carbon–cobalt oxide nanocomposite for high-performance enzymeless glucose sensor and supercapacitor applications. ACS Appl Mater Interfaces 2015;7:15812–20. https://doi.org/10.1021/acsami.5b04132.

[37] Sun C, Li F, Ma C, Wang Y, Ren Y, Yang W, Ma Z, Li J, Chen Y, Kim Y, Chen L. Graphene–Co_3O_4 nanocomposite as an efficient bifunctional catalyst for lithium–air batteries. J Mater Chem A 2014;2:7188–96. https://doi.org/10.1039/C4TA00802B.

[38] Enhessari M, Lachini SA. $CuMn_2O_4$ nanostructures: facial synthesis, structural, magnetical, electrical characterization and activation energy calculation. Int J Bio-Inorg Hybrid Nanomater 2019;8:39–45.

[39] Wang W. Facile hydrothermal synthesis of $ZnCo_2O_4$ nanostructures: controlled morphology and magnetic properties. J Mater Sci Mater Electron 2021;32:16662–8. https://doi.org/10.1007/s10854-021-06221-w.

[40] Jadhav HS, Roy A, Thorat GM, Seo JG. Facile and cost-effective growth of a highly efficient $MgCo_2O_4$ electrocatalyst for methanol oxidation. Inorg Chem Front 2018;5:1115–20. https://doi.org/10.1039/C7QI00736A.

[41] Djilali MA, Mekatel H, Mellal M, Trari M. Synthesis and characterization of $MgCo_2O_4$ nanoparticles: application to removal of Ni2+ in aqueous solution by adsorption. J Alloys Compd 2022;907:164498. https://doi.org/10.1016/j.jallcom.2022.164498.

[42] Valian M, Soofivand F, Yusupov MM, Salavati-Niasari M. Facile synthesis of $SrTiO_3$/$CoAlMnO_4$ nanocomposite: a rechargeable heterojunction photocatalyst with superior hydrogen storage capability. Int J Hydrogen Energy 2022;47:31624–37. https://doi.org/10.1016/j.ijhydene.2022.07.073.

[43] Masjedi-Arani M, Salavati-Niasari M. Facile precipitation synthesis and electrochemical evaluation of Zn_2SnO_4 nanostructure as a hydrogen storage material. Int J Hydrogen Energy 2017;42:12420–9. https://doi.org/10.1016/j.ijhydene.2017.03.055.

[44] Razavi FS, Hajizadeh-Oghaz M, Amiri O, Morassaei MS, Salavati-Niasari M. Barium cobaltite nanoparticles: sol-gel synthesis and characterization and their electrochemical hydrogen storage properties. Int J Hydrogen Energy 2021;46:886–95. https://doi.org/10.1016/j.ijhydene.2020.09.196.

[45] Honarpazhouh Y, Astaraei FR, Naderi HR, Tavakoli O. Electrochemical hydrogen storage in Pd-coated porous silicon/graphene oxide. Int J Hydrogen Energy 2016;41:12175–82. https://doi.org/10.1016/j.ijhydene.2016.05.241.

[46] Gholami T, Salavati-Niasari M, Varshoy S. Electrochemical hydrogen storage capacity and optical properties of $NiAl_2O_4$/NiO nanocomposite synthesized by green method. Int J Hydrogen Energy 2017;42:5235–45. https://doi.org/10.1016/j.ijhydene.2016.10.132.

[47] Masjedi-Arani M, Salavati-Niasari M. Novel synthesis of Zn_2GeO_4/graphene nanocomposite for enhanced electrochemical hydrogen storage performance. Int J Hydrogen Energy 2017;42:17184–91. https://doi.org/10.1016/j.ijhydene.2017.05.118.

[48] Sangsefidi FS, Salavati-Niasari M, Ghasemifard M, Shabani-Nooshabadi M. Study of hydrogen storage performance of ZnO–CeO_2 ceramic nanocomposite and the effect of various parameters to reach the optimum product. Int J Hydrogen Energy 2018; 43:22955–65. https://doi.org/10.1016/j.ijhydene.2018.10.082.

[49] Mehdizadeh P, Masjedi-Arani M, Amiri O, Al-Nayili A, Salavati-Niasari M. Eco-friendly sonochemistry preparation and electrochemical hydrogen storage of $LaCoO_3$/CoO/La_2O_3 nanocomposites. Fuel 2022;311:122544. https://doi.org/10.1016/j.fuel.2021.122544.

[50] Zinatloo-Ajabshir S, Salehi Z, Amiri O, Salavati-Niasari M. Green synthesis, characterization and investigation of the electrochemical hydrogen storage properties of $Dy_2Ce_2O_7$ nanostructures with fig extract. Int J Hydrogen Energy 2019;44:20110–20. https://doi.org/10.1016/j.ijhydene.2019.05.137.